 doi:10.20944/preprints201809.0605.v2

*Article*

# Adsorption of Carbon Dioxide into Amine Functionalized Ordered Mesoporous Materials

**Marcela N. Barbosa [1,*], Maria J. F. Costa [1], Maricele N. Barbosa [1], Valter J. Fernandes Jr. [1], Giancarlo R. Salazar-Banda [2], Ana C. F. Coriolano [3], Álvaro Reyes-Carmona [4], Enrique Rodríguez-Castellón [4] and Antonio S. Araujo [1,*]**

[1] Federal University of Rio Grande do Norte, Institute of Chemistry, Natal RN 59078-970, Brazil; mariacosta.ufrn@gmail.com (M.J.F.C.); maricelebarbosa@yahoo.com.br (M.N.B.); valter.ufrn@gmail.com (V.J.F.)
[2] Tiradentes University, Research and Technology Institute, Aracaju SE,49032-490, Brazil; gianrsb@gmail.com
[3] Potiguar University, Laureate International Universities, School of Information Technology and Engineering, Natal RN 59082-902, Brazil; catarina.coriolano@gmail.com
[4] University of Málaga, Faculty of Sciences, Department of Inorganic Chemistry, Crystallography and Mineralogy, Malaga CP 29071, Spain; alvarorcarmona@gmail.com (A.R.C.); castellon@uma.es (E.R.C.)
* Correspondence: mnbarbosa@gmail.com (M.N.B.), araujo.ufrn@gmail.com (A.S.A); Tel.: +55-84-3211-9240

**Abstract:** The adsorption of carbon dioxide on amino silanes-functionalized MCM-41 and SBA-15 materials is reported. The functionalization of mesoporous silicas was made by post-synthesis method, by impregnation of 3-aminopropyltriethoxysilane. The obtained materials were characterized by X-ray diffraction, scanning and transmission electron microscopies, nitrogen adsorption-desorption and X-ray photoelectron spectroscopy measurements. The carbon dioxide adsorption capacities for the samples were carried out under ambient pressures. The obtained results evidenced that amino-silanes with a terminal amine (–$NH_2$) were functionalized through covalent coupling of this group on the surface of the channels in the ordered mesoporous silica, meaning that the amine is anchored on the surface of the bigger pores of the MCM-41 and SBA-15 support. For functionalized materials, the $CO_2$ adsorption capacity of the AMCM-41 increased from 0.18 to 1.1 mmol·$g^{-1}$, whereas for ASBA-15, it was from 0.6 to 1.8 mmol·$g^{-1}$. The Lagergren kinetic algorithms were applied in order to validate the obtained results, evidencing the enhanced carbon dioxide adsorption capacity and stability of the functionalized ordered mesoporous molecular sieves.

**Keywords:** Adsorption; 3-Aminopropyltriethoxysilane; Carbon dioxide; Functionalization; Mesoporous silica; MCM-41; SBA-15

## 1. Introduction

The increase in the atmospheric carbon dioxide concentration is becoming a serious environmental problem. It is well known that the main human activity that emits $CO_2$ is the combustion of fossil fuels (coal, natural gas and oil) for energy and transportation, although certain industrial processes and land-use changes also emit $CO_2$. In the transition towards a more sustainable energy economy, fossil fuels are likely to remain the main source of global energy supply for the future [1,2]. Thus, the continuous use of fossil fuels is dependent on the reduction of $CO_2$ emissions. Improving the efficiency of energy utilization and increasing the use of low-carbon energy sources are considered to be potential ways to reduce $CO_2$ emissions. Recently, carbon capture and storage (CCS) techniques have been proposed as an emerging technology to effectively minimize $CO_2$ emissions [3].

 doi:10.20944/preprints201809.0605.v2



The most common technologies for $CO_2$ scrubbing from power plant flue gas are on the basis of adsorption, using liquid amines. The major drawbacks of these adsorbents are the large amount of energy required for regeneration, equipment corrosion, and solvent degradation in the presence of oxygen [4]. Therefore, extensive efforts have been directed to the development of alternative procedures for $CO_2$ capture, such as cryogenic technologies, adsorption or membrane based techniques [5,6]. Because of the low energy requirement, cost advantage, and ease of applicability over a relatively wide range of temperatures and pressures, adsorption separation attracts much interest.

The most important element of the chemical adsorption of $CO_2$ involves the design and development of a suitable adsorbent which consist of a porous support onto which an amine is attached [7]. The adsorption of carbon dioxide has been studied in various mesoporous materials including the MCM-41 and SBA-15 [8–11]. Groups of researchers have been trying to introduce amine groups into mesoporous silicas because of their elevated surface area. Polyethanolamine has been a modifying alternative for MCM-41 type materials, greatly improving the efficiency of the amine for $CO_2$ adsorption [12]. The $CO_2$ adsorption capacity of the modified adsorbent is 24 times higher than that of MCM-41. The use of amino groups anchored onto the support greatly reduces the potential toxicity of the process, minimize corrosion of equipment, and simplify the regeneration step. Mesoporous silicas with different pore size were modified by aminosilanes and $CO_2$ adsorption capacity was improved. However, (3-trimethoxysilylpropyl) diethylentriamine (TA) modified mesoporous silicas with small pores such as MCM-41 (2.9 or 3.1 nm) and SBA-15 (6.2 or 7.1 nm) were significantly decreased at high aminosilane density. In contrast, modified SBA-15 with a large pore (10.6 nm) exhibited further improvement of $CO_2$ adsorption capacity and amine efficiency [13].

According literature [14], mesoporous molecular sieves MCM-41 was modified by impregnation with polyethyleneimine (PEI) and $CO_2$ adsorption properties of these materials were found to depend on the kind and amount of the organic compound loaded. Grafted samples showed amine efficiencies in $CO_2$ capture up to 0.38 mol $CO_2$/mol N, leading to $CO_2$ uptakes ranging from 38.2 to 76.9 mg $CO_2$/g ads (pure $CO_2$, 45 °C, 1 bar) [14]. The key issue for adsorption separation is to develop an adsorbent with high $CO_2$ adsorption capacity and high $CO_2$ selectivity.

The aim of this works is to incorporate aminopropyltriethoxysilane (abbreviated as APTES) in the MCM-41 and SBA-15 mesoporous materials, in order to improve their adsorption capacities for $CO_2$, focusing to reduce the emissions greenhouse gases in the atmosphere. Differential of this work in relation to the others mentioned was the increase of the adsorption capacity, being used a simple system of low cost and in ambient conditions of temperature and pressure.

## 2. Materials and Methods

The ordered mesoporous molecular sieves MCM-41 and SBA-15 were synthesized by hydrothermal method according to the studies of literature [15,16]. Synthesis by the hydrothermal method was carried out in 200 mL Teflon containers introduced inside the system (autoclave stainless), under heating at 100 °C. In the synthesis of MCM-41, reagents precursors as silicon dioxide (Sigma-Aldrich) as a silicon source, sodium hydroxide as sodium source, cethyltrimethylammonium bromide (CTABr) as template structure and distilled water as solvent were used. An initial mixture with 11.6835 g silicon dioxide, 165 g distilled water and 3.7348 g sodium hydroxide was stirred for 2 h at 60 ° C and then it was added to an aqueous solution with 17.1125 g CTABr for 30 min to obtain a homogeneous mixture. Thereafter, this reactive hydrogel was transferred to a Teflon-lined stainless steel autoclave, which was kept at 100 °C during 96 h. A molar composition 1 CTMABr. 2 NaOH. 4 $SiO_2$. 200 $H_2O$ was used. The obtained material was filtered, washed, dried at 100 ° C for 4 h and calcined in $N_2$ and with air flow at 450 ° C for 2 h for the removal of the surfactant [15,16].

To obtain the SBA-15 mesoporous molecular sieve, the hydrogel was prepared with the following composition in grams: 10.4 TEOS / 4.8 P123 / 10 HCl / 174 $H_2O$. Other literature studies are able to obtain this material using Pluronic F127 and phenolic resin oligomers (resol) as precursors, however, the quantities in grams of these reagents were much higher compared to this work [17,18]. In this way, the choice of precursors and their quantities allowed lowering the synthesis cost. The

 doi:10.20944/preprints201809.0605.v2



mixture was stirred at 40 °C for 24 h, it was transferred to a Teflon-lined stainless steel autoclave, which were kept at 100 °C during 48 h. The precipitate was filtered, washed and dried at 100 °C overnight. To remove the structure-directing agent, the dried precipitate was calcined in air at 550 °C for 6 h.

The calcined MCM-41 and SBA-15 materials were functionalized by post-synthesis method, using a system reflux for impregnation of the APTES amine. Initially, the MCM-41 and SBA-15 were previously dried at 100 °C under $N_2$ flow during 2 h. Afterwards, 1 g of the mesoporous material was added to the mixture containing APTES (3 mL) and ethanol (30 mL), and submitted to reflux at 75 °C for 24 h. After, the products were filtered and washed several times with ethanol, and dried at 100 °C overnight. The obtained samples were labeled as AMCM-41 and ASBA-15, relative to MCM-41 and SBA-15 after grafting with 3-aminopropyl-triethoxysilane, respectively.

The X-ray diffraction (XRD) powder patterns were obtained with a Philips Xpert PRO apparatus using Cu K$\alpha_1$ radiation ($\lambda$ = 0.1540 nm) with Ge (111) monochromator working at 45 kV and 35 mA. All the measurements were made with a step size of 0.0167 degree in 30 min. Scanning electron microscopy (SEM) micrographs were obtained by using a JEOL SM 840 microscope, working at 15 kV. Samples were placed on an aluminum drum and metalized with a gold film using a JEOL Ion Sputter JFC 1100. Transmission electron microscopy (TEM) images were obtained with a Philips CM 200 microscope working at 100 kV. The measurements of energy dispersive X-ray spectroscopy were registered using an EDAX CM200ST probe based in a detector SiLi. The samples were dispersed in 2-propanol and dropped over a Cu grid.

Nitrogen adsorption-desorption measurements were performed at liquid $N_2$ temperature (-196 ºC) with an ASAP 2020 apparatus from Micromeritics. Before each measurement, samples were degassed by 12 h at 150 ºC and $10^{-2}$ Pa. The specific BET surface area ($S_{BET}$) was calculated using the BET equation, and the specific pore volume (Vp) was calculated at $P/P_0$ = 0.98. The pore size distribution was calculated following Kruk-Jaronie-Sayari method [19], taking the data of the desorption branch and assuming a cylindrical pore model.

The X-ray photoelectron spectroscopy (XPS) studies were realized by a Physical Electronic PHI 5700 spectrometer using non monochromatic Mg Kα radiation (300W, 15 kV, 1253.6 eV) for the analysis of the core level signals of C 1*s*, N 1*s*, O 1*s* and Si 2*p* with a hemispherical multichannel detector. The binding energy values were referenced to C 1*s* signal (284.8 eV). Shirley type background and Gauss-Lorentz curves were used to determinate the binding energy.

The $CO_2$ adsorption tests consisted of two steps: the activation and adsorption. A mass sample of ca. 100 mg were transferred to a glass sample holder, contained within the reactor, and subjected to activation step into a stream of $N_2$, approximately 150 mL $min^{-1}$ for 2 h at a temperature of 200 °C. After activation, the system was cooled to room temperature and then performed the adsorption step. Before starting the adsorption, the adsorbent was weighted again. The adsorption was carried out under atmospheric pressure and $CO_2$ flowing at 150 mL $min^{-1}$, at room temperature and variation in reaction time from 0 to 210 min. The adsorption capacity was calculated according to the weight variation observed to reach equilibrium as being equal to the ratio of the amount of $CO_2$ adsorbed by the adsorbent mass activated.

The adsorption kinetics were described by kinetic models of pseudo first and second-order. The linear form of the models is given by Lagergren equations (1) and (2) [20,21].

$$\log (q_e - q_t) = \log q_e - (K_1 / 2.303)\, t \quad (1)$$

$$t / q_t = 1 / (K_2\, q_e^2) + (1 / q_e)\, t \quad (2)$$

The values of $K_1$ can be obtained from the slope of the plot of log ($q_e$–$q_t$) versus $t$. The plot of $t$ / $q_t$ versus $t$ gives a linear relationship, allowing for computation of $q_e$ and $K_2$. The validity can again be tested by comparing values of $q_e$ obtained from the plots and from experiments [22].

Preprints (www.preprints.org) | NOT PEER-REVIEWED | Posted: 27 December 2018 doi:10.20944/preprints201809.0605.v2



## 3. Results and Discussion

### *3.1. Materials Characterization*

#### 3.1.1. X-Ray diffraction

The APTES-functionalized mesoporous molecular sieves MCM-41 and SBA-15, before and after surface modification, were characterized by XRD and the results are compared in Figure 1,2, respectively. The XRD patterns of MCM-41 (Figure 1a) and AMCM-41 (Figure 1b) are consistent with the literature, showing one large peak corresponding the plane (100), along with three small peaks of the planes (110), (200) and (210), which are typical features of MCM-41 materials [23,24]. The same behavior was observed with SBA-15 and ASBA-15 materials, that presented the diffraction peaks characteristic to mesoporous silicas in the plans (100), (110), and (200), as shown in Figure 2a,b for SBA-15 and ASBA-15, respectively. The structures of mesoporous materials after functionalization were preserved.

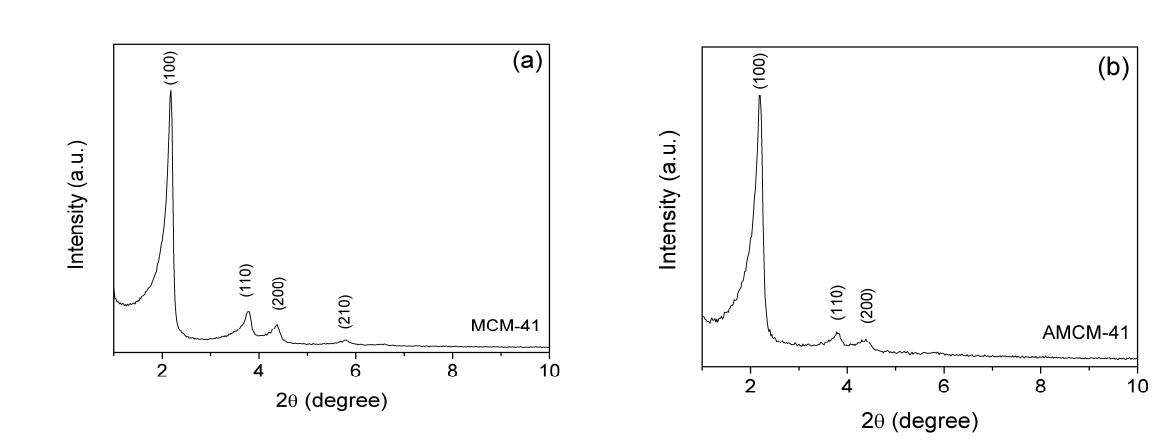


**Figure 1.** 1 Low-angle X-ray diffraction spectra of the synthesized materials: (**a**) MCM-41 and (**b**) AMCM-41 (MCM-41 after grafting with 3-aminopropyl-triethoxysilane).

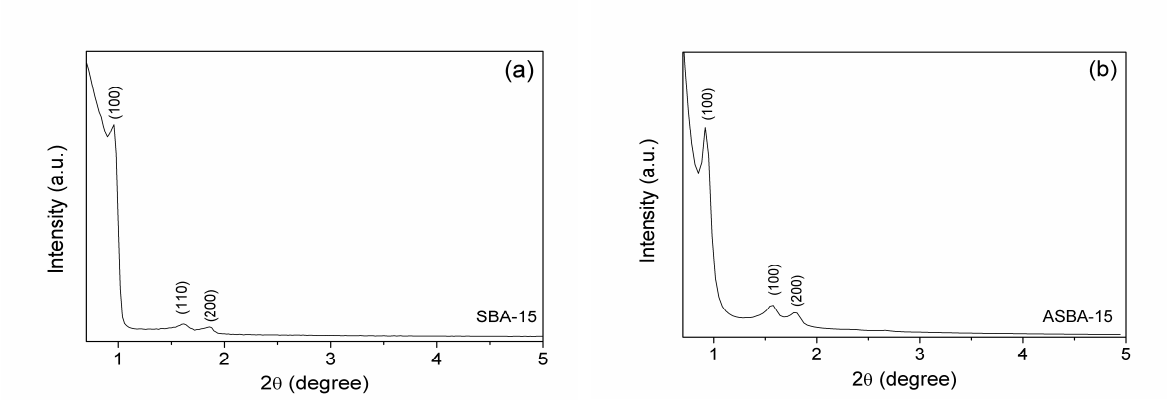


**Figure 2.** Low-angle X-ray diffraction spectra of the synthesized samples: (**a**) SBA-15 and (**b**) ASBA-15 (SBA-15 after grafting with 3-aminopropyl-triethoxysilane).

#### 3.1.2. SEM and TEM analysis

Analyses of SEM of the synthesized and functionalized samples are presented in Fig. 3. This technique was used in order to observe the morphology of materials obtained. According to the

 doi:10.20944/preprints201809.0605.v2



micrographs, the synthesized materials were formed by agglomeration of particles generally rounded. Moreover, for samples AMCM-41 and ASBA-15 (Figure 3b,d), the morphology of particles were similar when compared with the morphology of the synthesized material, MCM-41 and SBA-15 (Figure 3a,c).

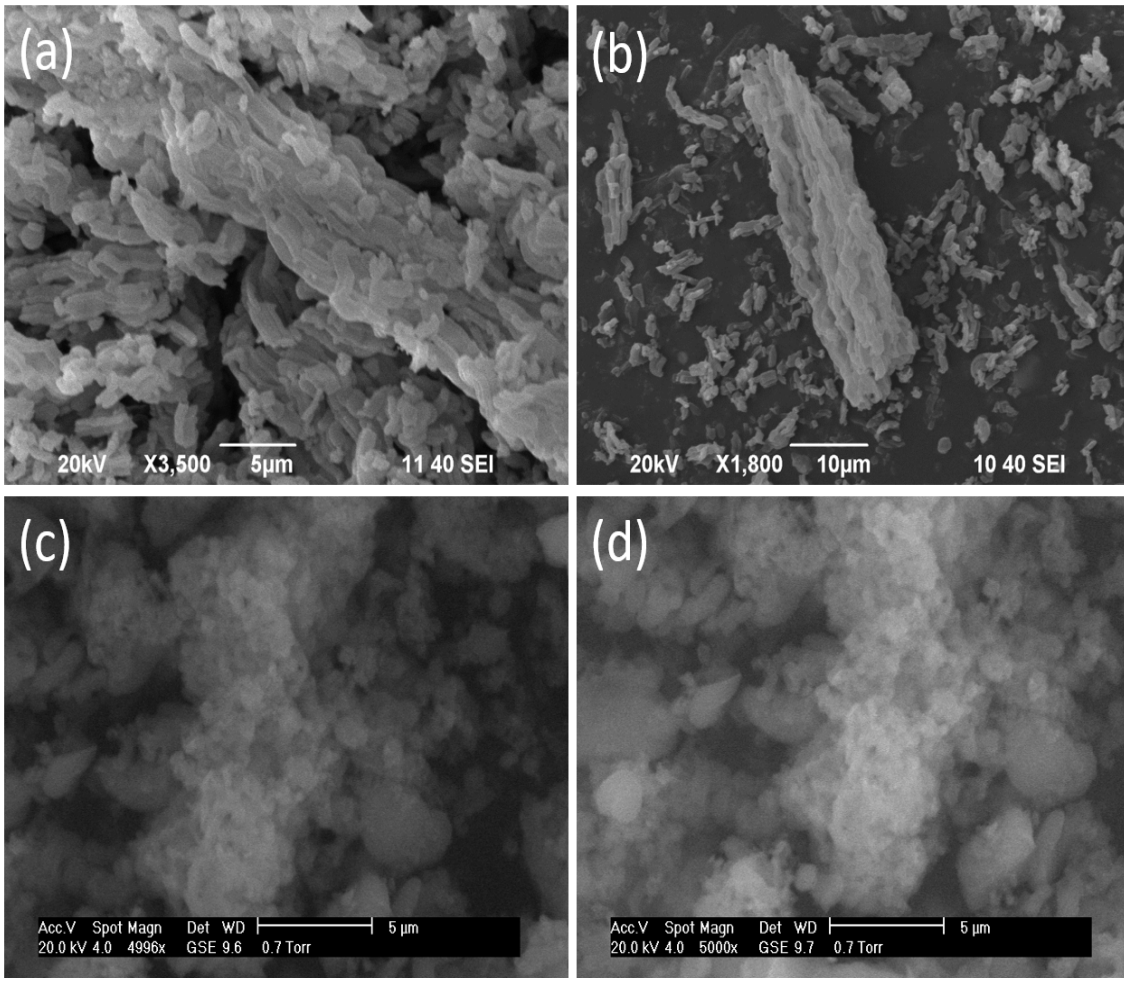


**Figure 3.** SEM images for samples (**a**) SBA-15 (×3.500), (**b**) ASBA-15 (×1.800), (**c**) MCM-41 (×4.996) and (**d**) AMCM-41 (×5.000).

The mesopores hexagonal structure of these materials cannot be observed through this analysis technique, because it does not provide an image resolution that reveals visually mesoporous hexagonal channels, as well as their lateral silica tubes. The technique that shows the exact structure for this type of material is TEM.

The TEM of the synthesized MCM-41 and SBA-15 materials (Figure 4a,c) showed the characteristic structures of mesoporous materials, since the formation of hexagonal ordered mesoporous and shows the high quality of material obtained. Besides the hexagonal mesoporous, we observed silica tubes formed in parallel. This result is directly correlated with the XRD technique, in which, the presence of the diffraction peak related to the plane (100) corresponds to the tubular channels formed by silica material. The same mesoporous structures were observed for samples functionalized AMCM-41 and ASBA-15 (Figure 4b,d), without compromising their structure even after functionalization with the amine. The functionalized materials maintained their hexagonal formation, as well as the ordering of their silica tubes.

 doi:10.20944/preprints201809.0605.v2



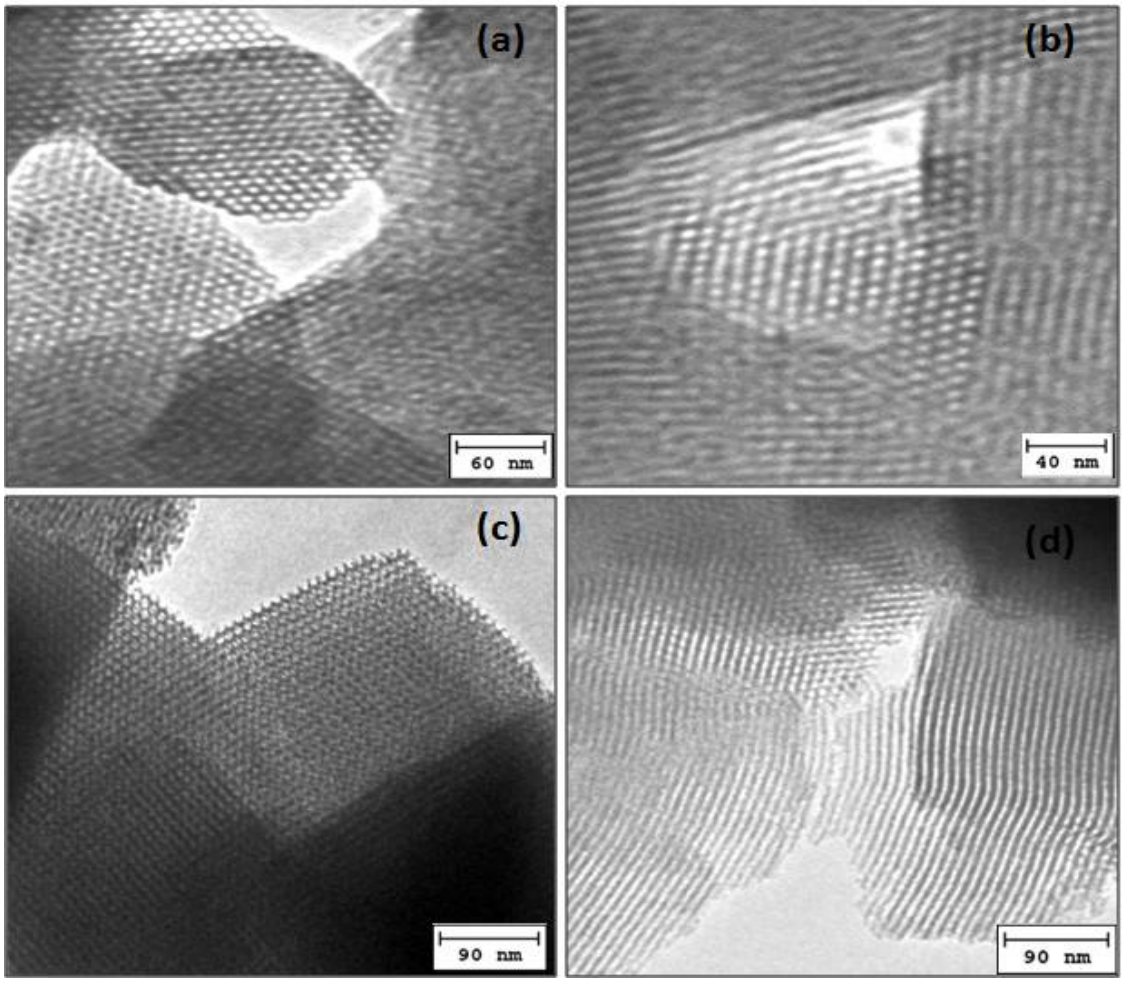


**Figure 4.** TEM image showing highly ordered, long-range hexagonal array of mesopores in the obtained materials before and after modification with amino silanes: (**a**) MCM-41, (**b**) AMCM-41, (**c**) SBA-15 and (**d**) ASBA-15.

### 3.1.3. $N_2$ Adsorption/Desorption Isotherms

Nitrogen adsorption/desorption isotherms of the materials studied are shown in Fig. 5. All the samples have the type-IV isotherm, following the recommendations of IUPAC [25] with a H1 hysteresis loop that is representative of mesoporous materials [26]. The isotherms of the samples have a sharp capillary condensation step. The parameters of the porous structure and XRD data are summarized in Table 1.

The MCM-41 and SBA-15 exhibit high values of surface area ($S_{BET}$), equivalent to 1070 and 713 $m^2 \cdot g^{-1}$, respectively. However, the functionalized samples, AMCM-41 and ASBA-15, had lower values regarding their textural properties when compared with pure materials, i.e. surface area of 666 and 465 $m^2 \cdot g^{-1}$, respectively.

Preprints (www.preprints.org) | NOT PEER-REVIEWED | Posted: 27 December 2018 doi:10.20944/preprints201809.0605.v2



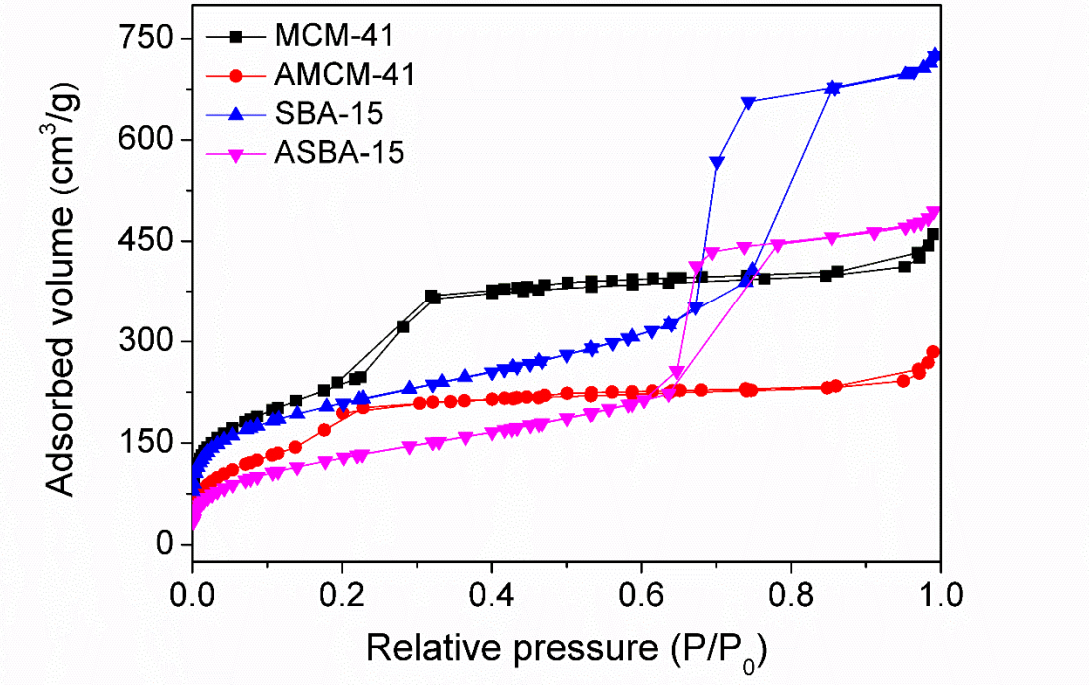


**Figure 5.** Nitrogen adsorption and desorption isotherms at -196 ºC for the MCM-41, AMCM-41, SBA-15 and ASBA-15 materials.

**Table 1.** Textural properties of the obtained materials before and after amino silanes surface modification.

| Materials | $a_0$ (nm) | Dp (nm) | Wt (nm) | Vp ($cm^3 \cdot g^{-1}$) | $S_{BET}$ ($m^2 \cdot g^{-1}$) |
|---|---|---|---|---|---|
| MCM-41 | 4.85 | 2.8 | 2.0 | 0.81 | 1070 |
| SBA-15 | 12.43 | 6.4 | 6.0 | 1.08 | 713 |
| AMCM-41 | 4.63 | 1.9 | 2.7 | 0.43 | 666 |
| ASBA-15 | 11.10 | 4.3 | 6.8 | 0.76 | 465 |

$a_0$: Lattice spacing, Dp: pore diameter, Wt: wall thickness (Wt = $a_0$ − Dp), Vp: pore volume, $S_{BET}$: surface area

For the MCM-41, AMCM-41 and SBA-15 materials, the Pore Size Distribution (PSD) analysis were obtained by the NLDFT method [27]. This is one of most adequate method for the PSD analysis of this mesoporous materials, which contains primary microporosity and a typical cylindrical geometry. The PSD graphics for the samples are shown in Figures 6(a)-(c). The micropore volume, micropore area and external surface area, are given in Table 2. The obtained data for MCM-41 and AMCM-41 samples, suggest that the amine functionalization decreased the external area, from 130 to 84 $m^2$ $g^{-1}$, and pore width, from 2.6 to 2.3 nm, respectively. For SBA-15, was obtained a maximum pore width of 7.0 nm, however values of 3.0 and 5.1 nm were observed. All these values being in the range of typical mesopores ordered materials.

Preprints (www.preprints.org) | NOT PEER-REVIEWED | Posted: 27 December 2018 doi:10.20944/preprints201809.0605.v2



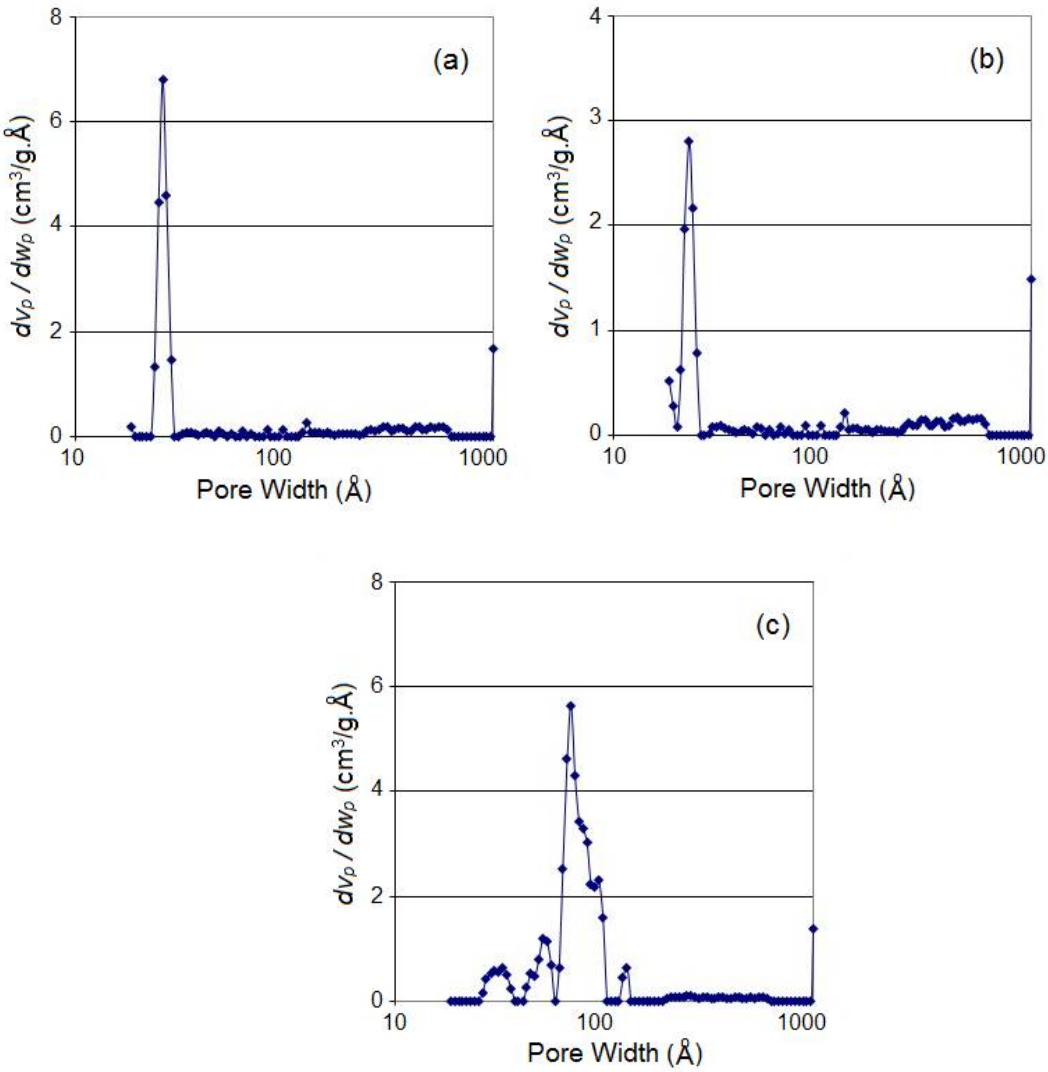


**Figure 6.** Pore size distribution obtained by NLDFT method for: (a) MCM-41; (b) AMCM-41; (c) SBA-15.

**Table 2.** Textural properties for synthesized materials.

| Materials | Total surface ($m^2$ $g^{-1}$) | Micropore area ($m^2$ $g^{-1}$) | External area ($m^2$ $g^{-1}$) | Vmic ($cm^3$ $g^{-1}$) | dw (nm) |
|---|---|---|---|---|---|
| MCM-41 | 878 | 748 | 130 | 0.50 | 2.6 |
| AMCM-41 | 783 | 699 | 84 | 0.28 | 2.3 |
| SBA-15 | 743 | 232 | 511 | 1.08 | 7.0 |

Vmic: Micropore volume; dw: Pore width

3.1.5. XPS analysis

The results concerning the characterization by XPS of the synthesized mesoporous materials are given in Table 3. According to the data, it was possible to obtain the atomic composition of the elements present in the materials. A much greater concentration of the nitrogen element was observed for the functionalized samples as compared to the non-functionalized samples, since the latter are not present in their elemental composition the nitrogen atom. The values for N and C

Preprints (www.preprints.org) | NOT PEER-REVIEWED | Posted: 27 December 2018 doi:10.20944/preprints201809.0605.v2



observed in MCM-41 and SBA-15 pure are considered interference rather than amine, since a significant difference was observed in these values when compared to AMCM-14 and ASBA-15. Therefore, this composition significant difference of N evidenced the presence of amine groups in these materials.

**Table 3.** Atomic concentrations of the elements in the synthesized materials.

| Materials | C 1*s* | N 1*s* | O 1*s* | Si 2*p* | C – $C_a$ / N | O / Si |
|---|---|---|---|---|---|---|
| MCM-41 | 4.95 | 0.18 | 64.1 | 30.8 | - | 2.08 |
| AMCM-41 | 17.3 | 2.25 | 53.4 | 27.0 | 5.49 | 1.97 |
| SBA-15 | 5.62 | 0.16 | 63.2 | 31.1 | - | 2.03 |
| ASBA-15 | 15.6 | 2.52 | 53.5 | 28.3 | 3.96 | 1.88 |

Figure 7 shows the N 1*s* core level spectra for the APTES functionalized samples, AMCM-41 and ASBA-15, respectively. These spectra can be decomposed in two contributions. The most intense peak at 399.4 ev is assigned to amine groups, and the second one, with lower relative intensity at 401.5 eV is due to protonated amine, being more pronounced in the case of sample ASBA-15.

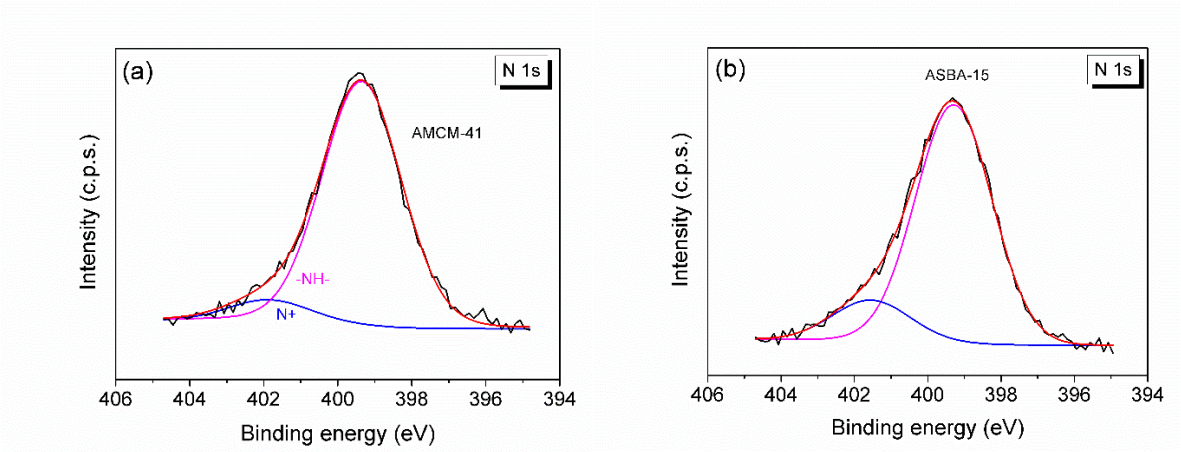


**Figure 7.** XPS spectrum N 1*s* of (**a**) AMCM-41 and (**b**) ASBA-15 samples.

### *3.2. $CO_2$ Adsorption*

To evaluate the potential of the obtained materials as adsorbents for $CO_2$ capture, Figure 8 shows the curves of adsorption of carbon dioxide materials. It was observed that the MCM-41 and SBA-15 showed low adsorption capacity for $CO_2$ compared to materials functionalized with APTES. The adsorption capacity of $CO_2$ increased despite the evident decrease in the specific surface area upon surface modification. This is related to an enhancement in surface affinity of the material with the adsorbent due to the incorporation of amino groups. The graph corresponding to the amount of $CO_2$ adsorbed versus time showed the isotherms for ASBA-15 and AMCM-41 samples, since their adsorption capacities have been improved from 0.6 and 0.1 mmol·$g^{-1}$, respectively, to reaching 1.8 and 1.0 mmol·$g^{-1}$. These adsorption improvements show the influence of amino groups in the structure of mesoporous materials, favoring the adsorption process.

In addition, these adsorption capacities were higher when compared with other similar works in the literature [28,29]. Another relevant factor is that the adsorption process was carried out at atmospheric pressure (1 atm) and at room temperature (30 °C), with a variation in adsorption time from 0 to 210 min. These conditions can be adjusted to tune the adsorption capacities, since changes in the adsorption temperature or pressure affects the amount uptake [30]. Note that the SBA-15 material shows a higher $CO_2$ uptake than that of MCM-41, despite the fact that its specific surface area is lower. This occurs because of the intrinsic microporosity of SBA-15 [31]. The positive effect of microporosity in the $CO_2$ uptake is well-documented elsewhere [32,33].

 doi:10.20944/preprints201809.0605.v2



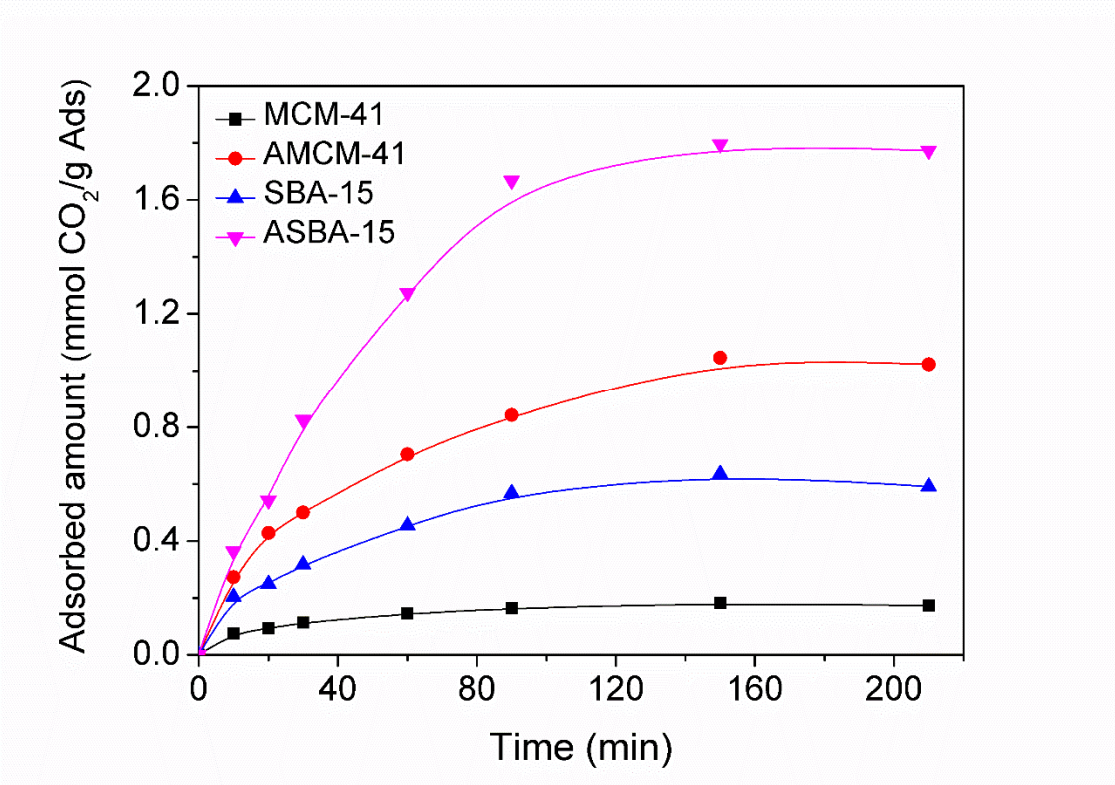


**Figure 8.** $CO_2$ adsorption capacities of the obtained materials, obtained at room temperature.

*3.3. Kinetic Study*

From the results of adsorption of $CO_2$ for various times, curves were constructed representing the kinetics of sorption of $CO_2$ by mesoporous materials. The graphs referring to kinetic models pseudo first-order, log ($q_e$–$q_t$) versus time, and the pseudo second-order, $t/q_t$ versus time, are shown in Fig. 9(a) and 8(b), respectively. Table 4 shows the kinetic parameters obtained by linear regressions of these graphs. Quantitative evaluation of models requires that the correlation coefficients are compared ($R^2$). It was observed that the $R^2$ values calculated for the kinetic model of pseudo second-order greater were than 0.99. Another relevant parameter was the calculated $q_e$ values. Since the calculated values of $q_e$ are greater than the experimental values of $q_e$, this one shows a consistency of results, otherwise, if the calculated values of $q_e$ are lower than the experimental values, they are not relevant. The results of adsorption did not fit the kinetic model of first-order by this fact. However, the $CO_2$ adsorption experiments were best fitted to the engine pseudo second-order, since this adjustment was confirmed by comparing of the experimental $q_e$ values with the calculated, which showed in good agreement.

Preprints (www.preprints.org) | NOT PEER-REVIEWED | Posted: 27 December 2018 doi:10.20944/preprints201809.0605.v2



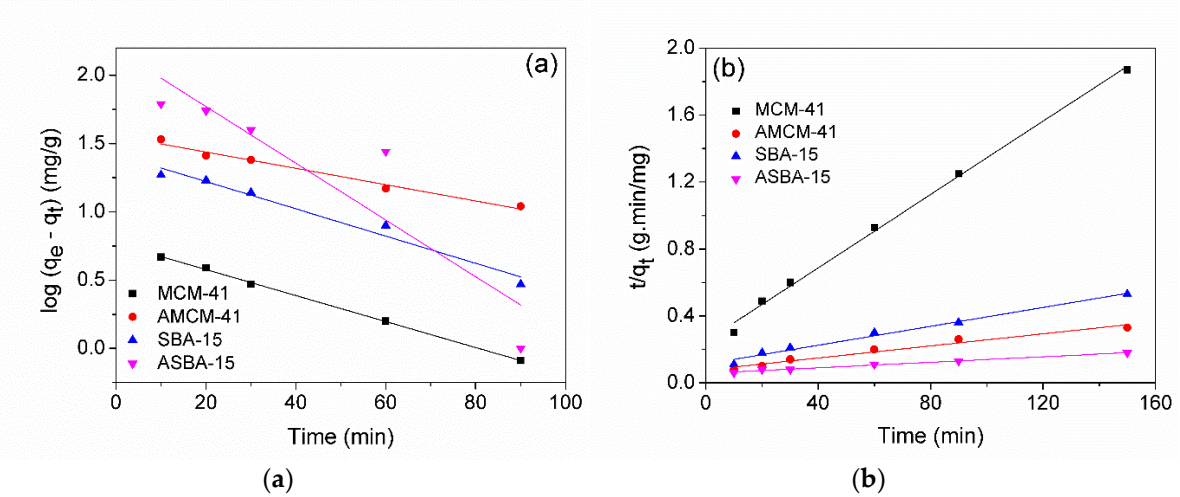


(a) (b)

**Figure 9.** Kinetic analysis of the $CO_2$ adsorption of materials studied at room temperature by (a) Lagergren pseudo first-order (LFO) equation and (b) pseudo second-order (PSO) equation.

**Table 4.** Kinetic parameters of the $CO_2$ adsorption of materials studied by Lagergren pseudo first-order equation and pseudo second-order equation.

| Kinetic | | MCM-41 | SBA-15 | AMCM-41 | ASBA-15 |
|---|---|---|---|---|---|
| First-order* | $K_1$ | 0.022 | 0.022 | 0.013 | 0.047 |
| | $R^2$ | 0.99 | 0.96 | 0.97 | 0.97 |
| | a | 0.76818 | 1.42023 | 1.55682 | 2.18579 |
| | b | −0.00953 | −0.00996 | −0.00597 | −0.02076 |
| | $q_e$ experimental | 8 | 28 | 46 | 79 |
| | $q_e$ calculated | 6 | 26 | 36 | 151 |
| Second-order** | $K_2$ | $6.2 \times 10^{-3}$ | $1.1 \times 10^{-3}$ | $6.2 \times 10^{-4}$ | $2.8 \times 10^{-4}$ |
| | $R^2$ | 0.99 | 0.99 | 0.99 | 0.99 |
| | a | 2.49319 | 1.12381 | 0.76129 | 0.56262 |
| | b | 0.10984 | 0.02821 | 0.01773 | 0.00843 |
| | $q_e$ experimental | 8 | 28 | 46 | 79 |
| | $q_e$ calculated | 9 | 35 | 56 | 118 |

*$\log(q_e - q_t) = \log(q_e) - (K_1/2{,}303)t$; **$t/q_t = 1/(K_2 q_e^2) + (1/q_e)t$ ; coefficients : a, b.

## 4. Conclusions

Amino silanes-functionalized mesoporous molecular sieves MCM-41 and SBA-15 type were prepared by post-synthesis functionalization via a facile reflux method. Through physico-chemical characterizations of the synthesized materials before and after modification with amine, it was possible to evaluate the efficiency of the functionalization method, showing the presence of amino groups in the structure of mesoporous molecular sieves, according to the XPS analysis. The $CO_2$ adsorption tests showed an increase in the amount of gas adsorbed on both samples containing amine, reaching 1.1 mmol·g$^{-1}$ for sample AMCM-41 and 1.8 mmol·g$^{-1}$ for sample ASBA-15. It was possible to compare the quantities adsorbed experimentally and theoretically through kinetic studies and thereby validate the adsorption experiments. The kinetic parameters obtained were best fitted to the kinetic model of second order, since the calculated values of $q_e$ were consistent compared with the experimental values, as well as the correction factor equal to 0.99. It is important to note that the $CO_2$ adsorption process was carried out at room temperature under atmospheric pressure. The results are relevant for such materials and can be improved by varying the condition of the adsorption process at different pressures and/or temperatures.

**Author Contributions:** Conceptualization on mesoporous materials for gas adsorption, M.N.B*. and M.N.B.; experimental methodology for synthesis and modification of adsorbents, M.J.F.C and J.R.S.B.; characterization of the materials by SEM, TEM and XPS, A.R.C. and E.R.C.; resources, some reagents and tools, V.J.F.; writing—original draft preparation, M.N.B*.; writing, review and editing, A.C.F.C. and A.S.A.

**Acknowledgments:** The authors thank the Brazilian Agency of Petroleum, Natural Gas and Biofuel (ANP), and National Council for Scientific and Technological Development (CNPq Brazil, Grant number 311136/2014-1), CAPES and Ministerio de Economía y Competitividad of Spain (CTQ2015-68951-C3-3-R from Spain and European FEDER funds for financial support. This work is result of a Brazil-Spain research cooperation.

**Conflicts of Interest:** The authors declare no conflict of interest.

## References

1. Beckman, E.J. Supercritical and near-critical $CO_2$ in green chemical synthesis and processing. *J. Supercrit Fluid* **2004**, *28*, 121–191.
2. Corfee-Morloj, J.; Höhne, N. Climate change: long-term targets and short-term commitments. *Global Environmental Change* **2003,** *13*, 277–293.
3. Zhou J.; Zhao, H.; Li, J.; Zhu, Y.; Hu, J.; Liu, H.; Hu, H. $CO_2$ capture on micro/mesoporous composites of (zeolite A)/(MCM-41) with $Ca^{2+}$ located: Computer simulation and experimental studies. *Solid State Sciences* **2013**, *24*, 107–114.
4. Du, R.; Feng, X.; Chakma, A. Poly(N,N-dimethylaminoethyl methacrylate)/polysulfone composite membranes for gas separations. *J. Membrane Sci.* **2006**, *279*, 76–85.
5. Tajnik, T.; Bogataj, L.K.; Jurač, E.; Lasnik, C.R.; Likar, J.; Debelak, B. Investigation of adsorption properties of geological materials for $CO_2$ storage. *Int. J. Energy Res.* **2013,** *37*, 952–958.
6. Yu, C.; Huang, C.; Tan, C. A review of $CO_2$ capture by absorption and adsorption. *Aerosol and Air Quality Research.* **2012**, *12*, 745–769.
7. Ünveren, E.E.; Monkul, B.O.; Sarıoglan, S.; Karademir, N.; Alper, E. Solid amine sorbents for $CO_2$ capture by chemical adsorption: A review. *Petroleum* **2017**, *3*, 37-50.
8. Carvalho, L.S.; Silva, E.; Andrade, J.C.; Silva, J.A.; Urbina, M.; Nascimento, P.F.; Carvalho, F.; Ruiz J.A. Low-cost mesoporous adsorbents amines-impregnated for $CO_2$ capture. *Adsorption* **2015**, *21*, 597–609.
9. Jing, Y.; Wein, L.; Wang, Y.; Yu, Y. Synthesis, characterization and CO2 capture os mesoporous SBA-15 adsorbents functionalized with melanine-based and acrylate-based amine dendrimers. *Micropor Mesopor Mater*. **2014**, *183*, 124–133.
10. Montagnaro, F.; Silvestre-Albero, A.; Silvestre-Albero, J.; Rodríguez-Reinoso, F.; Erto, A.; Lancia, A.; Balsamo, M. Post-combustion $CO_2$ adsorption on activated carbons with diferente textural properties. *Micropor Mesopor Mater*. **2015**, *209*, 157–164.
11. Vilarrasa-García, E.; Cecilia, J.A.; Bastos-Neto, M.; Cavalcante Jr, C.L.; Azevedo, D.C.S.; Rodríguez-Castellón, E. $CO_2/CH_4$ adsorption separation process using pore expanded mesoporous sílicas functionalizated by APTES grafting. *Adsorption* **2015**, *21*, 565–575.
12. Balaraman, E.; Gunanathan, C.; Zhang. J.; Shimon, L.J.W.; Milstein, D. Efficient hydrogenation of organic carbonates, carbamates and formates indicates alternative routes to methanol based on $CO_2$ and CO. *Nature Chem*. 2011, *3*, 609–614.
13. Hori, K.; Higuchi, T.; Aoki, Y.; Miyamoto, M.; Oumi, Y.; Yogo, K.; Uemiya, S. Effect of pore size, aminosilane density and aminosilane molecular length on $CO_2$ adsorption performance in aminosilane modified mesoporous silica. Microp. Mesop. Mater. **2017**, *246*, 158-165.
14. Sanz, R.; Calleja, G.; Arencibia, A.; Sanz-Pérez, E.S. $CO_2$ Capture with pore-expanded MCM-41 silica modified with amino groups by double functionalization. *Micropor Mesopor Mater*. **2015,** *209*, 165–171.
15. Araujo, A.S.; Jaroniec, M. Thermogravimetric monitoring of the MCM-41 synthesis. *Thermochimica Acta* **2000**, *363*, 175–180.
16. Zhao, D.; Huo, Q.; Feng, J.; Chmelka, B.F.; Stucky, G.D. Nonionic Triblock and Star Diblock Copolymer and oligomeric surfactant syntheses of highly ordered, hydrothermally stable, mesoporous silica structures. *J. Am. Chem. Soc.* **1998**, *120*, 6024–6036.

17. Qiang, Z.; Guo, Y.; Liu, H.; Cheng, S.Z.D.; Cakmak, M.; Cavicchi, K.A.; Bogt, B.D. Large-scale roll-to roll fabrication of ordered mesoporous materials using resol-sssisted cooperative assembly. *Appl. Mater. Interfaces* **2015,** *7*, 4306−4310.
18. Qiang, Z.; Gurkan, B.; Ma, J.; Liu, X.; Guo, Y.; Cakmak, M.; Cavicchi, K.A.; Vogt, B.D. Roll-to-roll fabrication of high surface area mesoporous carbon with process-tunable pore texture for optimization of adsorption capacity of bulky organic dyes. *Micropor Mesopor Mater.* **2016,** *227*, 57−64.
19. Jaroniec, M., Solovyov LA. Improvement of the Kruk-Jaroniec-Sayari method for pore size analysis of ordered silicas with cylindrical mesopores. Langmuir. 22(2006) 6757-6760.
20. Ayyappan, R.; Sophia, A.C.; Swaminathan, K.; Sandhya, S. Removal of Pb(II) from aqueous solution using carbon derived from agricultural wastes. *Process Biochemistry* **2005,** *40*, 1293–1299.
21. Yuh-Shan, H. Citation review of Lagergren kinetic rate equation on adsorption reactions. *Scientometrics* **2004**, *59*, 171–177.
22. Ho, Y.S.; McKay, G. Batch lead (II) removal from aqueous solution by peat: Equilibrium and kinetics. *Proc Safe Environ Protec*. **1999**, *77*, 165–173.
23. Beck, J.S.; Vartuli, J.C.; Roth, W.J.; Leonowicz, M.E.; Kresge, C.T.; Schmitt, K.D.; Chu, C.T.W.; Olson, D.H.; Sheppard, E,W.; McCullen, S.B.; Higgins, J.B.; Schlenker, J.L. A new family of mesoporous molecular sieves prepared with liquid crystal templates. *J. Am. Chem. Soc.* **1992**, *114*, 10834–10843.
24. Kresge, C.T.; Leonowicz, M.E.; Roth, W.J.; Vartuli, J.C.; Beck, J.S. Ordered mesoporous molecular sieves synthesized by a liquid-crystal template mechanism. *Nature* **1992,** *359*, 710–712.
25. Gregg, S.J.; Sing, K.S.W. *Adsorption, Surface Area, and Porosity*. 2nd ed. New York, Academic Press. **1982.**
26. Chareonpanich, M.; Nantangern, A.; Limtrakul, J. Short-period synthesis of ordered mesoporous silica SBA-15 using ultrasonic technique. *Mater Lett*. **2007,** *61*, 5153–5156.
27. Villarroel-Rocha, J.; Barrera, D.; Sapag, K. Introducing a self-consistent test and the corresponding modification in the Barrett, Joyner and Halenda method for pore-size determination. *Microp. Mesop. Mater.* **2014**, 200, 68–78
28. Ma, X.; Wang, X.; Song, C. Molecular basket sorbents for separation of $CO_2$ and $H_2S$ from various gas streams. *J. Amer. Chem. Soc.* **2009**, *131*, 5777–5783.
29. Xu, X.; Song, C.; Andrésen, J.M.; Miller, B.G.; Scarone, A.W. Preparation and characterization of novel $CO_2$ molecular basket adsorbents based on polymer-modified mesoporous molecular sieve MCM-41. *Micropor Mesopor Mater.* **2003**, *62*, 29–45.
30. Sanz-Pérez, E.S.; Dantas, T.C.M.; Arencibia, A.; Calleja, G.; Guedes, A.P.M.A.; Araujo, A.S.; Sanz, R. Reuse and recycling of amine-functionalized silica materials for $CO_2$ adsorption. *Chem. Eng. J.* **2017,** 308, 1021–1033.
31. Kruk, M.; Jaroniec, M.; Ko, C.H.; Ryoo, R. Characterization of the porous structure of SBA-15. *Chem. Mater.* **2000**, 12, 7, 1961-1968.
32. Ludwinowicz, J.; Jaroniec, M. Effect of activating agents on the development of microporosity in polymeric-based carbon for $CO_2$ adsorption. *Carbon* **2015**, 94, 673-679.
33. Liu, Y.; Liu, S.; Goncalves, A.A.S.; Jaroniec, M. Effect of metal-ligand ratio on the $CO_2$ adsorption properties of Cu-BTC metal-organic frameworks. *RSC Advances* **2018**, 8, 35551.